Modulation of spray droplet number density and size distribution by an acoustic field

Javier Achury and Wolfgang Polifke

Abstract

Multiple interactions may occur when a poly-disperse spray is exposed to an acoustic field. In the context of spray combustion instabilities, acoustic agglomeration, the formation of a droplet number density wave and the modulation of the droplet size distribution are interesting effects. A droplet number density wave, i.e. preferential concentration of droplets in space, may result from size-dependent, one-way momentum coupling between the acoustic field and the spray. The modulation of the droplet size distribution, which has been evidenced in the experimental work of Gurubaran and Sujith (AIAA 2008-1046), is thus a consequence of the droplet number density wave formation. In the present work, the mechanisms that produce these effects are simulated and analyzed in depth by means of computational fluid dynamics. The spray is modeled with both Lagrangian (particles mass-point approach) and Eulerian (continuous phase approach) descriptions. The particular Eulerian method used is a variant of the presumed density function method of moments, which allows to account for the effects of poly-dispersity, in particular the size-dependence of particle velocity. Both the Lagrangian and Eulerian models are validated against experimental data for spray dynamics and spray response to an acoustic field.

Introduction

In industrial systems that make use of sprays, there are important efforts to understand and characterize the spray dynamics and the spray response to oscillatory conditions of the carrier fluid. This is a critical aspect as the spray dynamics determines several features of the process or products. In sprays flames, for example, a steady droplet concentration is normally desired. Time-varying concentration of droplets lead to unsteady feed of fuel and, potentially, to a unstable combustion process. Periodic fluctuations of the fluid field, i.e. oscillating fields or acoustic waves, excite the spray periodically, producing an unsteady droplet concentration. This mechanism is clearly prejudicial and needs to be avoided. In other applications, interactions between a spray and periodic fluctuations of the fluid field may be beneficial. Acoustic agglomeration (AA), the mechanism that promotes particle collision and coalescence

due to the presence of velocity nodes (or attractors) in the acoustic field, is a good example. Recently, the use of acoustic standing waves to promote agglomeration of particulate material to ease filtration in exhaust systems (such as diesel engines) is being extensively investigated analytically, numerically and experimentally.[1]

The particular spray dynamics that results from the interaction with a pulsating or oscillating carrier flow is what we call here *spray response*. Although different scenarios of sprays interacting with unsteady flows have been studied experimentally,[2–5] by means of

Thermofluiddynamik, Technische Universität München, Garching, Germany

Corresponding author:
Wolfgang Polifke, Thermofluiddynamik, Technische Universität München, D-85747 Garching, Germany.
Email: polifke@tfd.mw.tum.de

computational fluid dynamics (CFD),[6,7] and analytically,[8,9] there is to the best of our knowledge no proper and comprehensive classification of different types of spray responses in the literature. The problem of making a rigorous classification lies in the fact that, depending on the scenario under investigation, various mechanisms are more or less dominant.

It should thus not come as a surprise that different studies draw very varied conclusions. Gajan et al.[4] present evidence that the fundamental spray response is the appearance of a number density (ND) wave. It is argued in that study that the origin of the ND wave is related to two factors: the atomization process itself and the fluctuating transport of small droplets. Gurubaran and Sujith have also performed experimental investigations in non-evaporating[2] and evaporating sprays[5] submitted to an axial acoustic field. They found that the spray velocity oscillates with the same frequency as the excitation signal, but out of phase. Droplets clustering and a maximum variation of 25% in droplet mean diameter were observed. The particle size distribution (PSD) was measured locally and averaged conditioned on the phase angle of the acoustic oscillation. A strong influence of the acoustic pressure amplitude on the modulation of the PSD was observed.

Guiliani et al.[7] performed experiments where both the liquid and the air in a liquid-fuel atomizer were pulsating. They concluded that, although relevant for technical combustion control, pulsations on the liquid phase do not affect considerably the PSD. However, the air pulsation produces a dense droplet front close to the injector exit. Such droplet concentration is formed and ejected periodically during the high-acceleration phase of the air velocity. A simplified Lagrangian CFD simulation for a set of poly-disperse particles was also performed in their work to illustrate the concept. It was concluded that the smaller droplets dominate the droplet ND wave formation, due to their low Stokes number. Chisty et al.[6] carried out a Lagrangian-drop/Eulerian-flow simulation study of a non-reacting spray in an acoustic field. A dense pocket of droplets appearing at an interval equal to the acoustic wavelength was found. Katoshevski et al.[8,9] attempted to study the droplet grouping phenomena analytically. They have proposed conditions under which droplet grouping may or may not occur, based on the solution of the equation of motion of a droplet excited by an acoustic wave with mean flow (only drag force was accounted for). This condition is related to how the droplets are attracted to a distance equal to the acoustic wavelength. Unfortunately, this analysis was performed for a combination of acoustic frequency and wavelength that is not realistic.

The remarkable variety of conclusions of the above-mentioned studies, the mixture of scenarios and the lack of knowledge of the role of the various parameters in the spray response have motivated the present investigation. We strive to clarify the role of each parameter by selecting simplified configurations of the spray (test cases) and use CFD methods to draw general conclusions, when possible. It is proposed that the spray response can be classified in terms of two effects: (1) AA and (2) generation of a droplet ND wave. Test cases corresponding to these effects are constructed and analyzed. A cross-validation that employs two approaches for sprays simulation, i.e. the Euler–Lagrange (EL) and the Euler–Euler (EE), is carried out for each case. We investigate the capabilities and limitations of the particular EE approach, the presumed density function Method of Moments (PMoM), to capture the aforementioned spray responses. Validation of the EL and EE models is also performed against the experimental results obtained by Gurubaran and Sujith[2] for a spray submitted to an axial acoustic field.

Mathematical model and considerations

Generally speaking, spray dynamics can be modeled by means of two descriptions, the EE and EL, where the carrier flow dynamics is expressed in Eulerian form in both. It is well known that each approach provides advantages and disadvantages in terms of mathematical modeling and computational cost. Despite the need of elaborate more mathematical models to account for poly-dispersity and poli-celerity for the EE case, this approach can be a cost-effective alternative.

Continuous phase equations

The Eulerian equations for the continuous phase are common for both approaches. In an incompressible flow, the continuity equation reads

$$\nabla \cdot \mathbf{u}_c = 0 \tag{1}$$

where $\mathbf{u}_c$ is the continuous phase velocity. The absence of source terms implies that small liquid volume fractions (α) are considered and droplets do not evaporate. The momentum equation reads

$$\frac{\partial \mathbf{u}_c}{\partial t} + \nabla \cdot (\mathbf{u}_c \mathbf{u}_c) = -\frac{1}{\rho_c} \nabla P + \frac{1}{\rho_c} \nabla \cdot \tau_c + \mathbf{g} + \frac{1}{\rho_c} \mathbf{M}_i \tag{2}$$

where P is the pressure, ρ_c the continuous phase density, $\mathbf{g}$ the gravity and τ_c the stress tensor. The source term $\mathbf{M}_i$ is the disperse phase (spray) momentum transferred from/to the continuous phase, where the subscript i stands for $i = L$ in the Lagrangian spray model and $i = E$ in the Eulerian.

For the one-dimensional test cases, the continuous phase velocity is imposed (one-way momentum

coupling). The general form of the excitation (varied according to the corresponding test case) is

$$u_c(x, t) = \hat{U}_c + \hat{u}_c \sin(2\pi f t) \cos(2\pi x/\lambda) \qquad (3)$$

where $\hat{U}_c$ is the mean flow velocity, f the frequency, $\hat{u}_c$ the amplitude of the velocity oscillation and λ the wavelength.

Since no thermal effects are contemplated, there is no energy equation and the continuous phase is assumed to be incompressible. The use of this incompressible approach is discussed in the validation section, as long as the validation problem can be approximated as acoustically compact.

Disperse phase equations

Lagrangian mass-point approach. In the Lagrangian framework, the spray model is comparatively simple. The equation of motion of a droplet with diameter D can be read as[10]

$$\frac{d\mathbf{u}_p}{dt} = \underbrace{\frac{3C_D}{4\gamma D}|\mathbf{u}_c - \mathbf{u}_p|(\mathbf{u}_c - \mathbf{u}_p)}_{\text{drag}}$$
$$+ \underbrace{\frac{1}{\gamma}\left(\frac{D\mathbf{u}_c}{Dt} - \nu_c \nabla^2 \mathbf{u}_c\right)}_{\text{undisturbed flow}} + \underbrace{\left(\frac{\gamma - 1}{\gamma}\right)\mathbf{g}}_{\text{gravity}} \qquad (4)$$

where $\mathbf{u}_p$ is the droplet velocity. Three forces have been considered here, the steady-state drag force, the undisturbed flow force and gravity. The drag coefficient $C_D = f_1 24/Re_p$ depends on the regime determined by the droplet Reynolds number, $Re_p = |\mathbf{u}_c - \mathbf{u}_p|D/\nu_c$, in the following way

$$f_1 = \begin{cases} 1 & Re_p < 1 \text{ Stokes flow} \\ 1 + 0.15 Re_p^{0.687} & Re_p < 800 \text{ Schiller and} \\ & \quad\quad\quad\quad\quad \text{Naumann} \end{cases}$$

Although the undisturbed flow force is composed by the pressure gradient the shear stress around the "absent" droplet,[10] with the help of the Navier–Stokes equations for an incompressible fluid, this force can be conveniently expressed only in terms of the fluid velocity field, as occurs in equation (4). For a gas-particle flow with large droplet and fluid density ratio $\gamma = \rho_p/\rho_c$, this force can be, in fact, neglected.

In the Lagrangian context, the momentum transfer from/to the continuous phase can be calculated as the local sum of the particles momentum variation along the Eulerian time step[a] $\Delta t_E = t_{out} - t_{in}$. For a given computational cell j, the source term due to momentum transfer becomes

$$\mathbf{M}_{L@cellj} = \frac{\sum_i \rho_p \frac{\pi}{6} D_i^3 \left(\mathbf{u}_{p,i,t_{out},cellj} - \mathbf{u}_{p,i,t_{in},cellj}\right)}{V_{cellj} \Delta t_E} \qquad (5)$$

Eulerian approach. The so-called PMoM is just one (among several) EE moment model for the description of a poly-disperse spray. A systematic derivation of the mathematical model of the PMoM is given in the work of Carneiro[11,12] or Dems.[13,14] Without detailing mathematical and statistical formalities of the method, the main idea is to resolve transport equations for the k moments $M^{(k)}$ of the number density function (NDF). These k transport equations

$$\frac{\partial}{\partial t} M^{(k)} + \nabla \cdot \left(M^{(k)} \mathbf{u}^{(k)}\right) = 0 \qquad (6)$$

are obtained after integrating the population balance equation[b] on the size spectrum. The moments of the NDF are the integrals

$$M^{(k)} = \int_0^\infty D^k f(D) \mathrm{d}D \qquad (7)$$

The NDF is defined as $f(D) = N_p \tilde{f}(D)/V$, where $\tilde{f}(D)$ is the probability density function (PDF)[15] (or particle NDF[11]) and V is the volume which contains a number of N_p droplets. $\mathbf{u}^{(k)}$ is the velocity (given in Eulerian coordinates) at which the corresponding k moment of the NDF is transported, formally

$$\mathbf{u}^{(k)} = \frac{1}{M^{(k)}} \int_0^\infty \mathbf{u}(D) D^k f(D) \mathrm{d}D \qquad (8)$$

The moments $M^{(k)}$ provide statistical information of the evolution of the NDF in time and space. Thus, once the set of k equations (6) are resolved in the problem domain, $f(D)$ can be reconstructed if a presumed function is selected. Two requirements are fundamental in order to build an appropriate PDF: (1) the presumed function must represent a typical spray droplet size distribution (DSD) and (2) provide an analytical solution of the integral (7). Although, there are several possible candidates, the gamma distribution fulfills these two requirements and is selected here. Thus, $f(D) = C_0 D^{q-1} \exp(-D/p)/p^q \Gamma(q)$, being the gamma function $\Gamma(q) = \int_0^\infty r^{(q-1)} e^{-r} \mathrm{d}r$. Three parameters ($C_0$, p and q) define exactly the shape of $f(D)$ and any of its moments can be explicitly calculated by means of

$$M^{(k)} = C_0 \frac{\Gamma(q+k)}{\Gamma(q)} p^k \qquad (9)$$

A set of moments needs to be selected to perform the reconstruction. For the gamma function, three consecutive moments are required, then

$$p = \frac{M^{(k_m+2)}M^{(k_m)} - \left(M^{(k_m+1)}\right)^2}{M^{(k_m)}M^{(k_m+1)}} \qquad (10)$$

$$q = \frac{(k_m+1)\left(M^{(k_m+1)}\right)^2 - k_m M^{(k_m+2)}M^{(k_m)}}{M^{(k_m+2)}M^{(k_m)} - \left(M^{(k_m+1)}\right)^2} \qquad (11)$$

$$C_0 = \begin{cases} \frac{M^{k_m}}{p^{k_m}\prod_{l=0}^{k_m-1}(q+l)} & \text{if } k_m \in N^+ \\ M^{(0)} & \text{if } k_m = 0 \end{cases} \qquad (12)$$

k_m is chosen depending on which quantity one wants to ensure conservation. Making $k_m = 0$ or $k_m = 1$ ensures the conservation of number of particles per unit volume $M^{(0)}$ or volume fraction $\alpha \ (= \pi M^{(3)}/6)$, respectively.

Nevertheless, there is still an issue regarding the transport velocities for the moments $\mathbf{u}^{(k)}$, since they are not yet in closed form. This is in fact the main matter of the approach for poly-celerity of the method. For the third moment $M^{(3)}$, a disperse phase momentum equation can be set in order to resolve $\mathbf{u}^{(3)}$

$$\frac{\partial}{\partial t}\left(M^{(3)}\mathbf{u}^{(3)}\right) + \nabla \cdot \left(M^{(3)}\mathbf{u}^{(3)}\mathbf{u}^{(3)}\right) = -\frac{1}{\rho_d}\mathbf{S} + \frac{\mathbf{g}}{\rho_d M^{(3)}} \qquad (13)$$

$\mathbf{u}^{(3)}$ is assumed to represent the mean spray velocity. $\mathbf{S}$ is the integral over the size spectrum of the individual contribution of momentum transfer from the particle to the continuous phase, or vice versa, via drag, then

$$\mathbf{S} = 18\mu_c\left(M^{(1)}(\mathbf{u}^{(1)} - \mathbf{u}_c) + 0.15 M^{(1.687)} \right. \\ \left. \times \left(\frac{|\mathbf{u}^{(1)} - \mathbf{u}_c|}{\nu_c}\right)^{0.687}(\mathbf{u}^{(1.687)} - \mathbf{u}_c)\right) \qquad (14)$$

This expression is obtained after integrating the drag force indicated in equation (4) on the size spectrum. It contains both the linear (Stokes) and non-linear (Schiller and Naumann) law for drag (see "Lagrangian mass-point approach" section). The corresponding momentum transfer term in equation (2) becomes $\mathbf{M}_E = 6/\pi\mathbf{S}$, which confers the momentum coupling between the two phases.

For the rest of the transport velocities $\mathbf{u}^{(k)}$, a fast Eulerian method is used, the so-called *relaxation approach*, which is inspired in the concept of Eulerian equilibrium proposed by Ferry and Balachandar[16,17]

and developed for the PMoM approach by Carneiro.[11] The Eulerian equilibrium offers a fast way to estimate the particle velocity based only on its characteristic time response $\tau_p = \gamma D^2/18\nu_c$ and the continuous phase velocity. If this particle velocity is integrated on the size spectrum and a reference velocity is chosen $(\mathbf{u}^{(3)})$, the following equation is obtained to estimate the k moments transport velocities

$$\mathbf{u}^{(k)} \approx \mathbf{u}_c + \frac{\tau^{(k)}}{\tau^{(3)}}\left(\mathbf{u}^{(3)} - \mathbf{u}_c\right), \quad \tau^{(k)} \propto \frac{M^{(k+2)}}{M^{(k)}} \qquad (15)$$

Although, this approach results very efficient computationally, important assumptions have been made. Our task is to identify if they are restrictive or not for sprays in oscillating flows.

The set of equations (1), (2), (6) and (13) are resolved using a customized OpenFOAM® code, which is based on a finite volume discretization. A first-order integration schema has been used to resolve equation (4), based also in an existing OpenFOAM library.

Problem description of the test cases

The test cases set-up is represented in Figure 1. In which, for "Acoustic agglomeration" section, all droplets are placed at initial time (no injection), while for the "ND wave formation" and "Modulation of the DSD" sections, a continuous injection of droplets is implemented.

Acoustic agglomeration

Consider a population of droplets that is positioned in a section of a one-dimensional channel, as represented in Figure 1.

For the Lagrangian representation 12,000 particles[c] are placed uniformly in space, which produces a constant initial ND profile. The droplets diameter follow a Gamma density distribution with parameters $p = 6 \cdot 10^{-6}$ and $q = 6$.
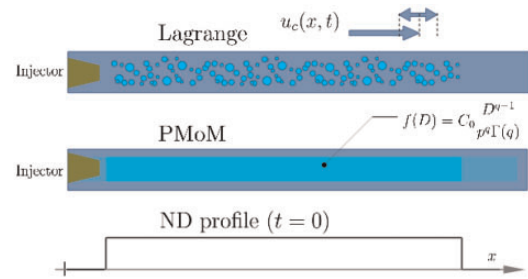

Figure 1. Illustration of the test case. Initial ND profile for the AA case.

The corresponding Eulerian model can be constructed based on the adopted density function. The zero-moment $M^{(0)}$, which represents the droplets ND, is calculated to equal the assumed initial droplet ND of the Lagrangian case. The first and second moment of the NDF are also calculated and set uniformly within such region.

An acoustic standing wave may be described a velocity field for the continuum $u_c(x,t) = \hat{u}_c \sin(2\pi ft) \cos(2\pi x/\lambda)$ and the spray response to such oscillatory motion is evaluated. In order to understand the flow physics of the mechanism of AA, consider the motion of a droplet during the first half of a cycle, say. A droplet is displaced to a position, where the intensity of the acoustic oscillation is larger, if it is initially at a position where the slope of the wave amplitude is positive (the second half of a wave length, say). Conversely, if the initial position is at a position where the slope is negative, the particle is displaced to point with reduced oscillation amplitude. During the second half of cycle, the reverse effect is observed, such that net droplet displacement after one cycle towards the closest velocity node results. This occurs for each acoustic cycle, independent of the initial droplet position. Therefore, all droplets are continuously attracted towards the standing wave velocity nodes, producing peaks of the ND at those locations.

This mechanism of AA is clearly recovered by both CFD model formulations (see Figure 2): a droplet ND profile composed by a series of U-shape intervals is established in the x domain. This profile becomes more prominent as the time advances and the accumulation rate, which could be measured as the rate at which these peaks grow, augments if the amplitude of the excitation ($\hat{u}_c$) increases and diminishes if the frequency (f) augments. Nevertheless, in an ideal gas, the potential increment of the accumulation rate by decreasing the frequency is compensated by larger wavelengths, as long as frequency and wavelength are coupled by the speed of sound ($\bar{c} = \lambda f$). In fact, it can be stated that the dimensionless number controlling the AA mechanism is the acoustic displacement (or acoustic Mach number) $M_a = \hat{u}_c/\lambda f$. In this mechanism, the ND of droplets increases or decreases continuously in time at each point with almost imperceptible oscillations.

The corresponding PMoM simulation of the equivalent problem captures qualitatively the evolution of the ND profile (dotted lines in Figure 2). However, the development of the ND profile is slower than in the Lagrangian reference case (dashed lines of Figure 2). This suggests that the way in which the transport velocity of the zero moment $u^{(0)}$ is estimated (relaxation approach, see above), is under-predicting the amplitude and/or the phase angle with respect to the excitation u_c.
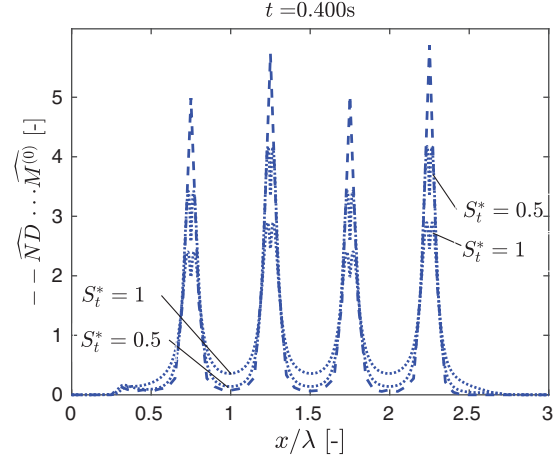
Figure 2. Normalized ND profile obtained with Lagrange mass-point approach (– – –) and PMoM approach (· · ··) after 100 acoustic cycles. Frequency $f = 250$ Hz, wave length $\lambda = 0.4$ m, oscillation amplitude $\hat{u}_c = 15$ m/s, Stokes numbers $S_t^* = 0.5$ and 1, respectively.
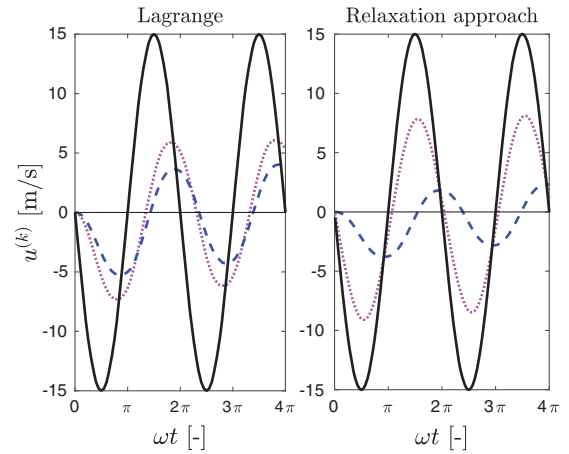
Figure 3. Time signals of u_c (———), $u^{(3)}$ (– – –) and $u^{(0)}$ (· · ·) at the velocity anti-node ($x/\lambda = 1.5$), calculated with the results of the Lagrangian case (left) and PMoM prediction with relaxation approach ($S_t^* \to \infty$) (right).

In order to analyze to what extent the predictions obtained by the relaxation approach are accurate, the transport velocities $u^{(0)}$ and $u^{(3)}$ are reconstructed from the Lagrangian results according to equation (8)[d] at the most critical point, which in this case is the velocity anti-node. At this location, the excitation velocity is maximal and the droplet ND tends to zero, which is evidently a very critical scenario to evaluate the PMoM performance. The time series of excitation u_c and responses ($u^{(0)}$ and $u^{(3)}$) calculated from the Lagrangian case are represented in Figure 3 (left), where it can be appreciated that there is a small phase

angle between the moments transport velocities. The phase lag between the zero and third moment velocity ($u^{(0)}$ and $u^{(3)}$) is over-predicted at this point if the relaxation approach is used, see Figure 3 (right), which is reflected in a delayed droplet ND profile formation. In order to correct this over-prediction, an improvement of the relaxation approach for oscillating conditions of the fluid is proposed in this work. We call it *relaxation approach with limited inertia*.

Relaxation approach with limited inertia

One of the fundamental premises of the Eulerian equilibrium method (which derives the relaxation approach) is that it is suitable only for small particle relaxation times (τ_p). This is due to the particle velocity **u** is expanded in Taylor series in τ_p but truncated in the first-order term. This makes that the method implicitly presumes that the size–velocity correlation follows a quadratic function of the size, in the form: $\mathbf{u}(D) \approx \mathbf{u}_c + \kappa D^2$. On the other hand, for particles immersed in oscillating flows, it is known that for large Stokes numbers ($S_t = \tau_p f$), particles are almost insensitive to the flow oscillation due to their large inertia.[18] This, in fact, can be seen in Figure 4, where the droplets velocity at a velocity anti-node are plotted against their size, for two phase angles of the fluid oscillation $\phi = 0$ and $\phi = \pi$.

So, there is a conflict between the unbounded (quadratic) nature of the implicit size–velocity correlation of the relaxation approach for large sizes and the bounded particle response expected for large S_t (large D). Two potential alternatives may resolve this conflict: (1) a higher order expansion in τ_p or (2) bounding the quadratic function of the size–velocity correlation in the "standard" relaxation approach. The latter alternative is employed here as the extension of high-order terms requires a complex mathematical treatment involving total derivatives and gradients of the velocity field $\mathbf{u}_c$[16] and is not easily implementable in the PMoM context. If a critical Stokes number S_t^* (where the particles

become less sensitive to the flow oscillation) is identified, the corresponding critical diameter is

$$D^* = \sqrt{\frac{18\nu_c S_t^*}{f\gamma}} \tag{16}$$

A piecewise size–velocity correlation (bounded) can be adopted saying that

$$\mathbf{u}(D) \approx \begin{cases} \mathbf{u}_c + \kappa D^2 & \rightarrow \text{ if } D \leq D^* \\ \mathbf{u}_c + \kappa D^{*2} & \rightarrow \text{ if } D > D^* \end{cases} \tag{17}$$

Combined with the definitions of the incomplete gamma functions

$$\Gamma_1(r, q) = \int_0^r r^{q-1} e^{-r} \mathrm{d}r \text{ and}$$

$$\Gamma_2(r, q) = \int_r^\infty r^{q-1} e^{-r} \mathrm{d}r$$

the following corrected expression for the relaxation approach is obtained

$$\mathbf{u}^{(k)} \approx \mathbf{u}_c + \frac{\Gamma(q+3)}{\Gamma(q+k)}$$
$$\times \frac{\Gamma_1\left(\frac{D^*}{p}, q+k+2\right) + \left(\frac{D^*}{p}\right)^2 \Gamma_2\left(\frac{D^*}{p}, q+k\right)}{\Gamma_1\left(\frac{D^*}{p}, q+5\right) + \left(\frac{D^*}{p}\right)^2 \Gamma_2\left(\frac{D^*}{p}, q+3\right)} \left(\mathbf{u}^{(3)} - \mathbf{u}_c\right) \tag{18}$$

in which only a new input S_t^* must be specified. In the limiting case for $S_t^* \rightarrow 0$ then $\mathbf{u}^{(k)} \approx \mathbf{u}^{(3)} \forall k$ and for $S_t^* \rightarrow \infty$, the standard relaxation approach (equation (15)) is obtained.

Employing the limited inertia schema decreases this phase angle, as it can be seen in Figure 5. This improves significantly the agreement of the droplet ND profile formation of the PMoM approach with respect to the Lagrangian one, as the delay of the former is reduced. This can be appreciated in Figure 2 for two critical Stokes numbers S_t^*.

A closer look for the size–velocity correlation ($u(D)$) at the velocity anti-node (see Figure 4) supports properly the need of using the correction for large particle sizes in oscillating excitations. Although droplets continuously leave the plot as the time lapses, the shape of the evolving size–velocity correlation is maintained. Clearly, this function can be properly approximated by a quadratic function only for small droplets sizes (see dotted lines in Figure 4), but may cause over- or under-predictions up to some critical sizes D^* (or S_t^*). In fact, the values of S_t^* used here ($S_t^* = 0.5$ and $S_t^* = 1$) are not arbitrary, they correspond to the interval where
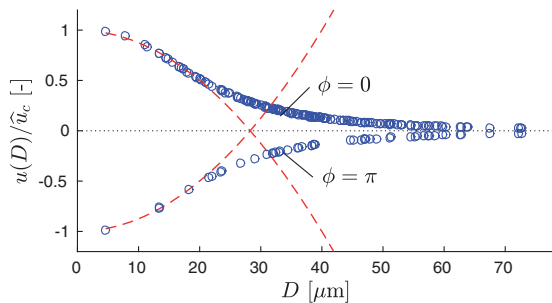
Figure 4. Size–velocity correlation at the velocity anti-node ($x/\lambda = 1.5$). Circles represent Lagrangian droplets.
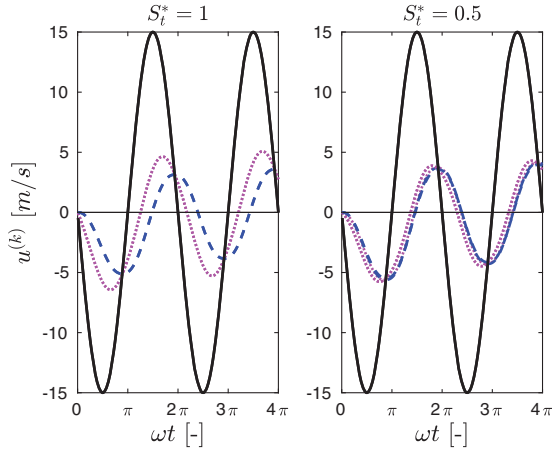
Figure 5. Time signals of u_c (———), $u^{(3)}$ (— — —) and $u^{(0)}$ ($\cdots$) at the velocity anti-node ($x/\lambda = 1.5$). The correction for large diameters ("Relaxation approach with limited inertia" section) has been employed. $S_t^* = 1$ (left) and $S_t^* = 0.5$ (right). $f = 250\,$Hz.
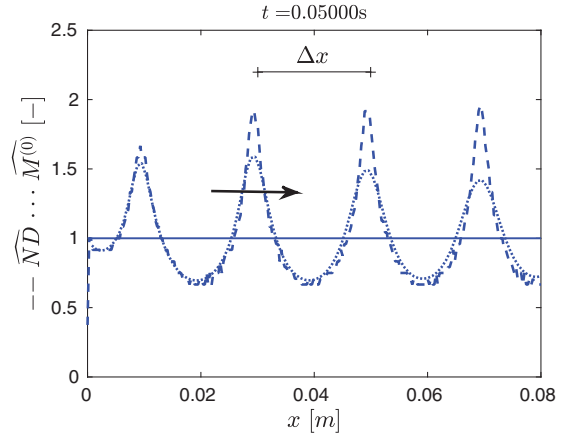

Figure 6. ND wave formation for a mono-disperse spray ($D = 25\,\mu$m) interacting with an oscillating velocity field with mean flow. Injection takes place at $x = 0$. The straight line represents the ND profile without excitation ($\hat{u}_c = 0$). The normalized droplet ND wave ($\widehat{ND}$) in the presence of excitation is obtained by means of the Lagrangian simulation (— — —) and $\widehat{M^{(0)}}$ by the Eulerian approach ($\cdots$). Wave length $\lambda = \infty$, frequency $f = 250\,$Hz, mean flow velocity $\hat{U}_c = 5\,$m/s and oscillation amplitude $\hat{u}_c = 2.5\,$m/s.

the size–velocity correlation has the inflection point.[18] The relaxation approach with limited inertia relieves this over- or under-predictions because it recovers the bounded nature of the size–velocity correlation.

The wavelength λ is a key parameter for AA. Note that, in principle, if $\lambda \to \infty$ the ND would not suffer any distortion, since droplets would not have any attractor. This result implies that a distortion of the ND profile in oscillating flows ($\lambda \to \infty$) can be expected only if this scenario is changed. We consider in the next section, a continuous injection of droplets interacting with an oscillating flow with mean velocity.

ND wave formation

The continuous injection of droplets (mono-disperse spray with $D = 25\,\mu$m) and mean flow in the forced field $\hat{U}_c$ are now introduced in the model. We study the case where the acoustic wavelength is infinite $\lambda = \infty$, to differentiate it from mechanisms linked to acoustics (finite λ), thus, the excitation becomes: $u_c(x, t) = \hat{U}_c + \hat{u}_c \sin(2\pi f t)$. Since a mono-disperse population is considered, a special Eulerian spray solver is implemented (method of classes for one class), in which only the transport equation for the volume fraction (α) is resolved (equation (13) for $M^{(3)}(= \alpha 6/\pi)$) and the momentum transfer of the mono-disperse population of droplets is calculated according to

$$\mathbf{S} = \frac{108\mu_c\alpha}{\pi D^2}(\mathbf{u} - \mathbf{u}_c)\left(1 + 0.15\left(\frac{|\mathbf{u} - \mathbf{u}_c|D}{\nu_c}\right)^{0.687}\right) \quad (19)$$

The continuous injection of droplets in an oscillating population generates a ND wave at the injection area which is transported downstream by the mean flow $\hat{U}_c$. The mechanism is simple, each injected droplet moves at the mean flow component of the velocity $\hat{U}_c$ while it is transported back and forth due to the oscillating component $\hat{u}_c$. Since this occurs continuously in time, the whole cloud of droplets oscillates. If the rate of droplet injection is constant, more droplets are appended to the population when the velocity of the cloud oscillation is zero and the peak of the wave is formed.

In Figure 6, both the droplet ND and $M^{(0)}$ waves are normalized with respect to the value without excitation and represented for $t = 0.05\,$s. The ND wavelength, indicated in Figure 6, can be estimated by $\Delta x = \hat{U}_c/f$. By carrying out simulations where the parameters are varied (results not shown here), it can be concluded that the amplitude of the ND wave grows when $\hat{u}_c$ or f increase, but decreases if the size (D), densities ratio (γ) or mean flow ($\hat{U}_c$) augment.

Modulation of the DSD

The ND wave formation in a poly-disperse injection of droplets is reflected as a local modulation of the DSD in time, as can be appreciated in Figure 7 (top). Any given point sees an undulating droplet ND profile traveling at a velocity $\hat{U}_c$. The modulation of the size distribution is the result of the modulation of each droplet class, according to the effect described in "ND wave
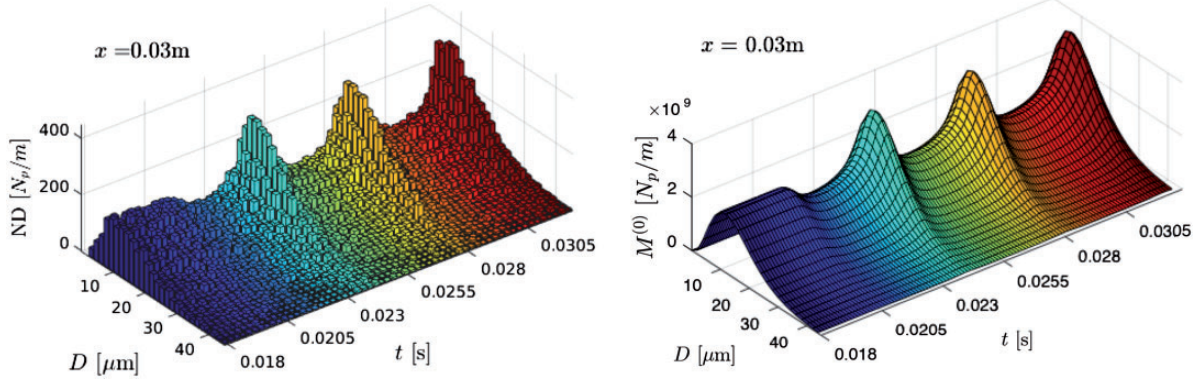
Figure 7. Left: modulation of the DSD at $x = 0.03$ m. Right: reconstructed function of the PMoM simulation.
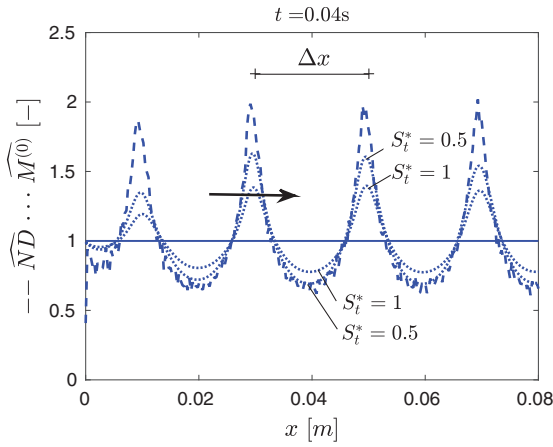
Figure 8. Poly-disperse spray response obtained with Lagrange mass-point approach (- - -) and PMoM ($\cdots$). The continuous line indicates the droplet ND profile before the system is excited. The droplets are injected at $x = 0$ m. $\lambda = \infty$, $f = 250$ Hz, $\hat{U}_c = 5$ m/s and $\hat{u}_c = 2.5$ m/s. The droplet ND wave is formed at the injection plane and transported downstream by the mean velocity $\hat{U}_c$.
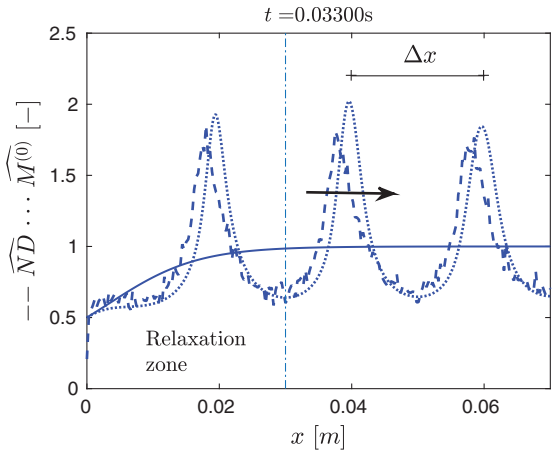
Figure 9. ND wave formation of the poly-disperse spray with relaxation, obtained with Lagrange (- - -) and PMoM ($\cdots$) for $S_t^* = 0.5$. The continuous line indicates the droplet ND profile before the excitation starts. The droplets are injected at $x = 0$ m. $\lambda = \infty$, $f = 250$ Hz, $\hat{U}_c = 5$ m/s and $\hat{u}_c = 2.5$ m/s.

formation'' section. Taking into account that no interactions among droplets are considered, i.e. collisions or coalescence, the main features of the droplet ND wave formation, presented in "ND wave formation" section, are preserved for the poly-disperse case: the amplitude of the local DSD modulation grows with $\hat{u}_c$ and f, the period of modulation is $1/f$ and the U-shape of the size distribution modulation is linked to the U-shape obtained for the droplet ND profile. The reconstructed DSD obtained with the PMoM model (Figure 7 (bottom)) is also modulated and corresponds to the Lagrangian prediction, the mechanism is properly captured by the PMoM.

The droplet ND wave for the Lagrangian model and the PMoM approach for two values of the critical

Stokes number (S_t^*) are presented in Figure 8. Note that good predictions are achieved only if (again) the relaxation approach with limited inertia is used (see the dotted lines in Figure 8). Likewise the results obtained in "Acoustic agglomeration" section, a close match is reached for $S_t^* \approx 0.5$. Then, the correction schema is also important here because the amplitude of the ND wave would be drastically underestimated by the standard relaxation approach ($S_t^* \to \infty$).

Phase lag of the modulated DSD

Due to the size-dependent relaxation that each droplet experiments, a phase lag in the modulated DSD is expected for large diameters. This situation is more evident if a relative velocity in the droplets injection is introduced in the previous test case ($\hat{U}_c \neq u_p(x = 0)$).

For this scenario, the spray relaxes until it reaches an equilibrium velocity. The interval where this occurs, called here *relaxation zone*, is delimited by a vertical line in Figure 9. As long as the spray velocity relaxes, the ND increases, which is represented with the solid line in Figure 9.

If an oscillation in the gas field is imposed ($\hat{u}_c > 0$), a number particle density pocket is formed. This dense pocket, is transported downstream by the mean flow producing the modulation of the DSD, following the same mechanism described in "Modulation of the DSD" section. Since each droplet class relaxes differently according to its size, a phase lag in the modulated DSD (see arrows in Figure 10) develops. This effect is well predicted by the Lagrangian simulation (Figure 10 (left)) but poorly captured by the PMoM as shown in
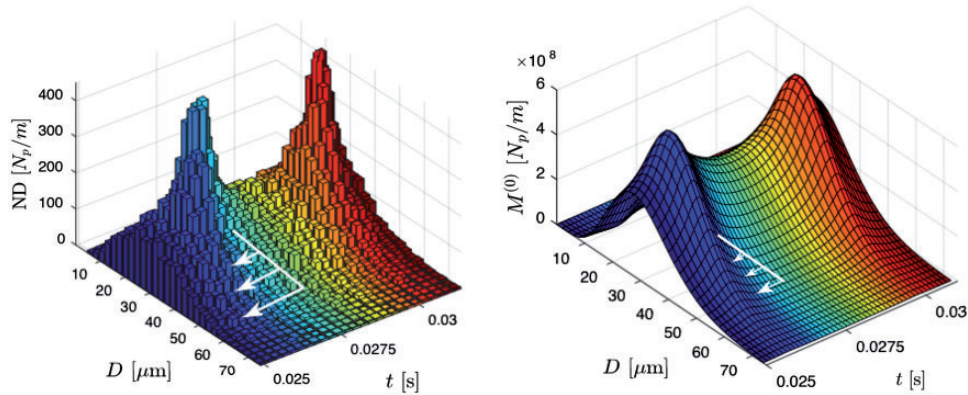
Figure 10. Local modulation of the DSD and phase lag (arrows) due to the droplets relaxation. Lagrange (left) and PMoM for $S_t^* = 0.5$ (right) prediction.
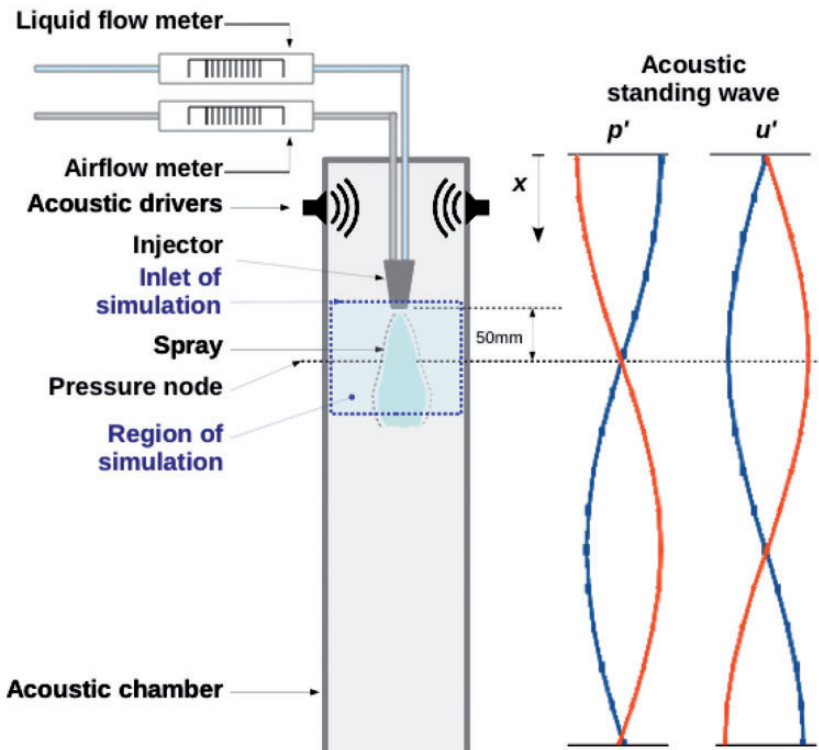
**Figure 11.** Schema of the experimental setup.[2]

Figure 10 (right). The inability of the PMoM approach to treat the dynamics of each droplet class independently results evident for this scenario. Nevertheless, it has been shown that the PMoM approach works fine for relatively compact size intervals, where the phase lag is expected to be small.

Comparison with experiment

As a validation case, the experimental setup of Gurubaran and Sujith[2] has been taken, which is represented in Figure 11. It consists of an injector fed by a liquid and a gas line, placed inside of an acoustic chamber. Four acoustic drivers, placed on the top of the channel, are synchronized to produce an acoustic standing wave, which interacts with the spray. The location of the injector is adjusted in such a way that the solid cone spray reaches one of the standing wave pressure nodes. In that position, the largest acoustic velocity amplitude is produced.

Our CFD model comprises the reduced section where the spray develops. We assume this section to be acoustically compact, as its length is small compared to the acoustic wavelength, and therefore, the gas is presumed to be incompressible. This is advantageous in terms of both solver formulation and boundary conditions treatment for acoustic waves.[19] By doing so, we automatically discard AA (as described in "Acoustic agglomeration" section) as a dominant mechanism. This is reasonable because the flow velocity in the spray axis is large, the acoustic velocity amplitude is relative small and only few acoustic cycles pass between the transport of particles from the injector to the pressure node. Therefore, the intensity of droplets
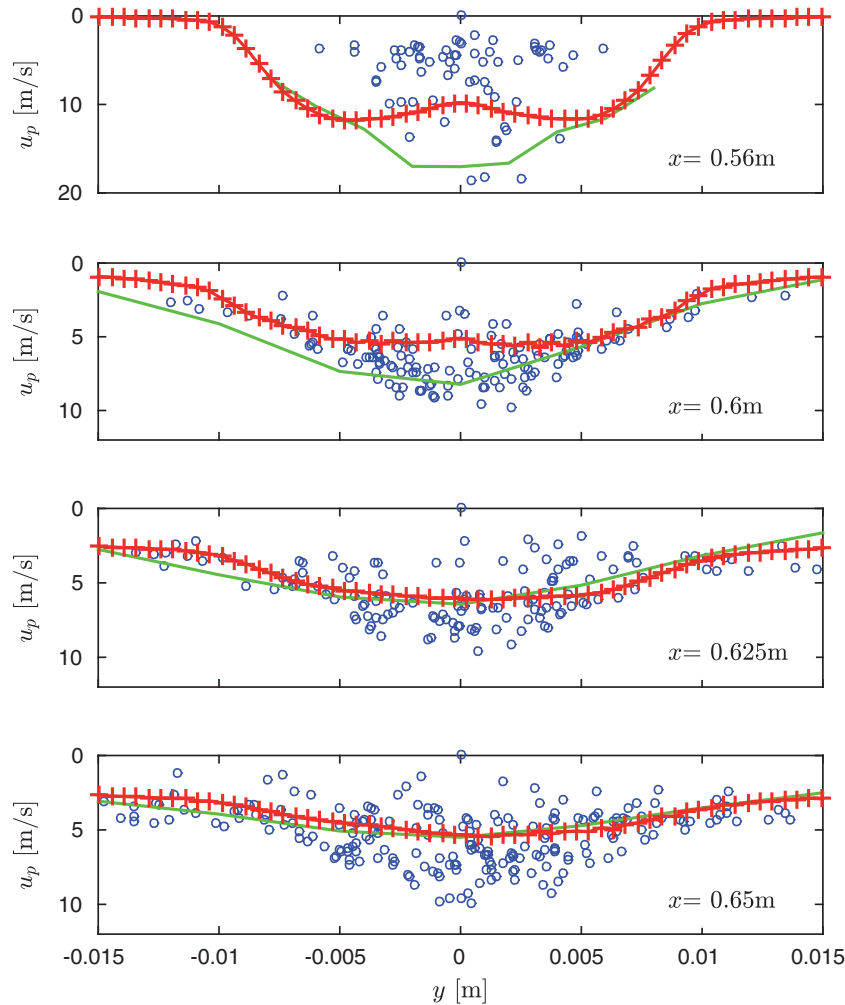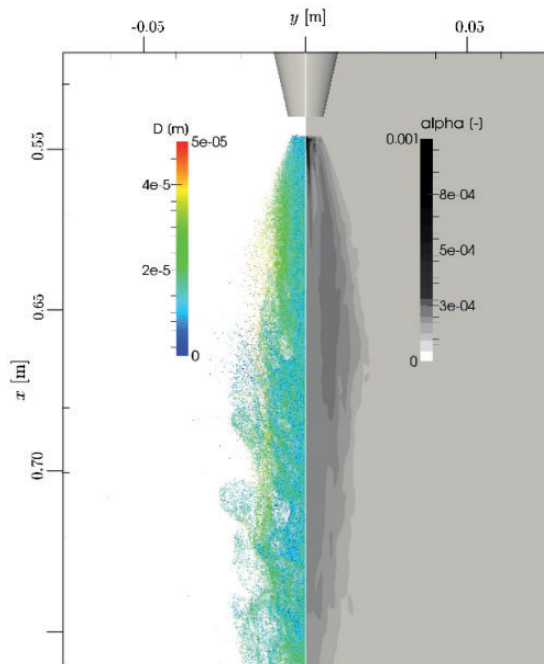

Figure 12. Spray axial velocity immediately downstream of the atomizer exit, which is located at $x = 0.55$ m. Experimental value (———), Lagrangian velocity of droplets crossing a thin layer at the corresponding section (instantaneous, not post-processed) (0) and PMoM (+).
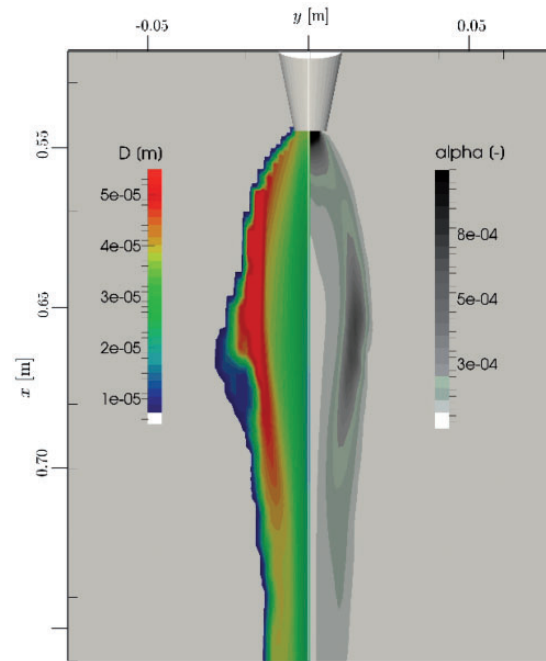
clustering due to AA is small in this case. Thus, we want to prove that the DSD modulation evidenced in the experiment can be explained by the mechanism of droplet ND wave formation.

Boundary conditions of the CFD model are approximated in the following manner: for the Lagrangian case, an injection of droplets was implemented in the code. It consists in a series of points of injection on the atomizer exit, where droplets are appended at a given velocity emulating the spray velocity profile measured experimentally. The diameter of each injected particle follows the discrete DSD measured at the pressure node. The rate of injected particles and the air entrance at the injector exit were estimated to satisfy the global liquid phase load ($\alpha = 0.0025$), which corresponds to the spray with a Weber number of $We = 33.1$.[e] The concept of parcel or super-particle has been used here, which means that one computational parcel represents a number of particles n_p. In order to satisfy the liquid phase load with 420 points of injection, n_p is 10 in our case. The distribution of the air velocity and liquid volume fraction on the injection patch are uncertain boundary conditions, as they were not measured experimentally. Both were initially assumed to be constant through the injection patch, but, in order to get a better approximation, they were varied in a series of iterations of the simulations to obtain approximately the spray velocity profile at $x = 0.65$ m (pressure node location). This time-consuming step was required for a

good description of the spray dynamics before an excitation was applied. For the PMoM simulation, the droplet velocity field at the atomizer exit was mapped directly as the $\mathbf{u}^{(3)}$ profile. The corresponding moments of the selected DSD combined with the required liquid injection rate ($M^{(3)} = 6\alpha/\pi = 0.0048$) were calculated and set as fixed values on the injection patch.
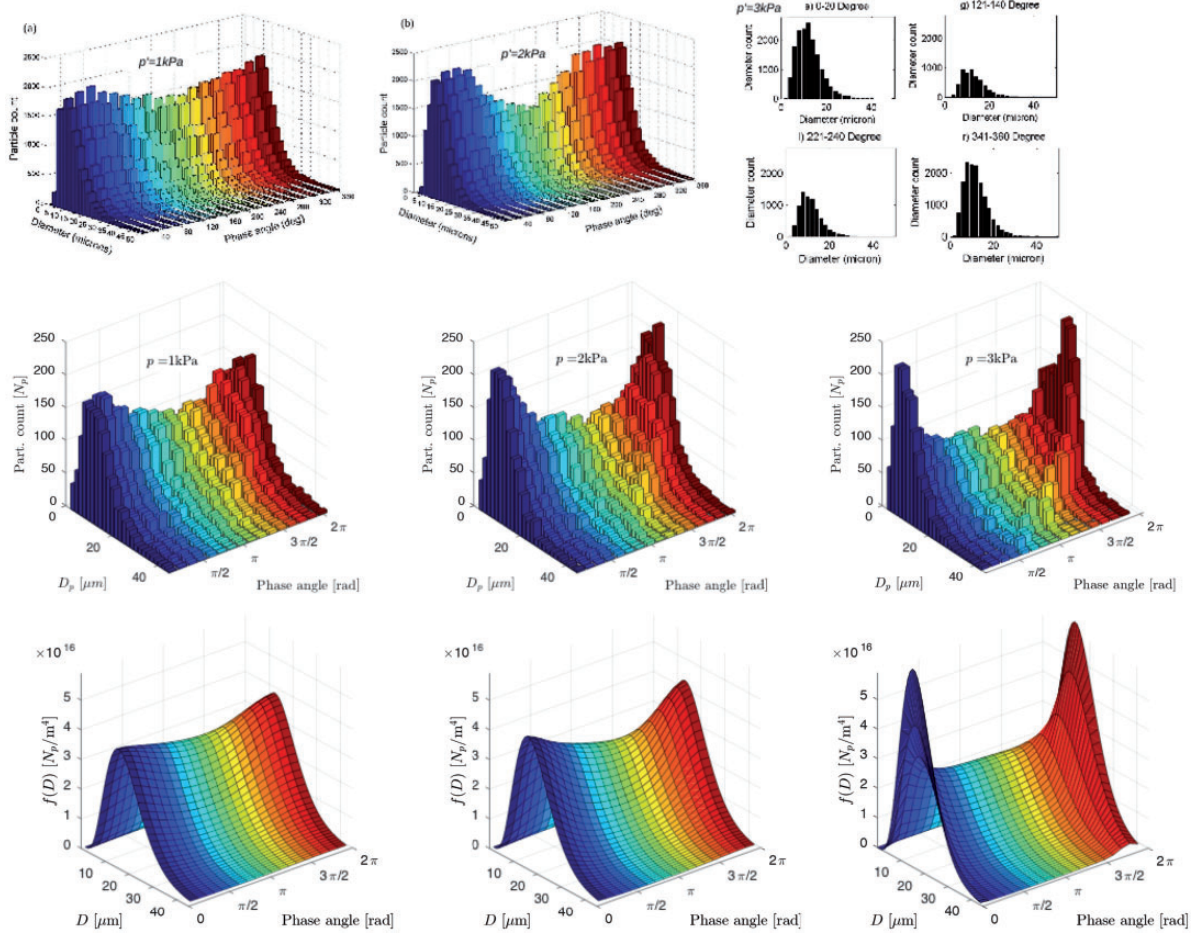

Figure 14. Sauter mean diameter ($D_{32} = M^{(3)}/M^{(2)}$) (left) and volume fraction (right) of the spray without excitation. PMoM model.

Figure 13. Droplet size (left) and volume fraction (right) of the spray without excitation. EL model.
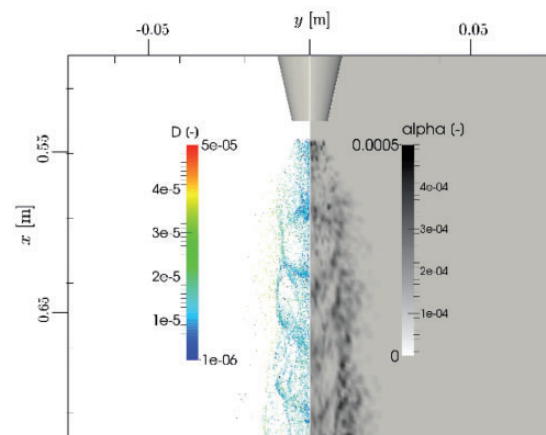
Figure 15. Droplet size (left) and volume fraction (right) in a thin cross-sectional area of the spray with excitation. $p' = 3$ kPa, $f = 250$ Hz. EL model.

Figure 16. Phase-locked DSDs of droplets at the pressure node ($x = 0.05$ m from the atomizer exit) for different amplitudes of excitation (from left to right $p\prime = 1$, 2 and 3 kPa, respectively). Experimental measurement (top[21]), Lagrangian mass-point approach (middle) and PMoM reconstruction (bottom).

For the aforementioned volume fraction, two-way momentum coupling is expected and the system of equations [(1), (2), (4)] and [(1), (2), (6), (13)] are resolved for the Lagrangian mass-point and PMoM approach, respectively.

First, the spray without an imposed acoustic wave is simulated. The x-component of the spray velocity u_p at axial planes $x = 0.56$, 0.6, 0.625 and 0.65 m, respectively, is presented in Figure 12. Adaptation of the profiles of volume fraction and air velocity on the injection patch resulted in a good match between experiment and computation, in particular at the most downstream location. This level of agreement allows meaningful comparison of DSD modulation in the presence of oscillations, see below. Note that for the Lagrangian simulation, individual particle velocities are plotted (0) without further post-processing. This choice was made because due to the limited number of computational particles, any averages would not be robust. In Figure 13, a thin cross-sectional area of the spray

simulated with the Lagrangian mass-point approach can be appreciated. Although the spray is relatively dense at the injection plane, spreads quickly. Thus, the two-way momentum coupling between the spray and carrier gas remains reduced to a relatively small volume at the tip of the conical shape. The droplets with larger sizes tend to concentrate at the spray periphery, as shown by the experiment. The corresponding spray model simulated by means of the PMoM is presented in Figure 14. A non-physical concentration at the spray edge is observable. A similar issue is reported by Bo and Watkins[20] who affirm that this occurs because moments of higher order tend to zero much faster than low-order moments. This accumulation at the spray edge, although uncomfortable for the view, seems not to influence the dynamics of our points of interest located at the spray axis. The mean diameter also grows in the spray periphery.

The excitation is applied as a uniform air velocity fluctuation (which is equivalent to excite the pressure)

around the cone of injection. A small mean flow velocity was also imposed (0.1 m/s), in accordance to the experiment characterization. The structure that the spray develops when the acoustic excitation is applied ($p' = 3$ kPa and $f = 250$ Hz) is shown in Figure 15 for a thin cross-sectional area.

It can be appreciated that dense droplet clusters are formed at the injection zone and transported downstream with the local fluid velocity. The cluster extinguishes progressively downstream, as the air flow velocity decreases.

The DSD was measured experimentally at several positions along the spray axis using phase Doppler particle size analyzer (PDPA)/laser Doppler velocimetry (LDV), but we focus on measurements performed at the pressure standing wave node in particular. In this technique, two lasers intersect forming a small probe window at the measurement location. A droplet crossing this window produces an interference pattern that can be used to determine its size and velocity. Each droplet crossing the probe window contributes to the respective bin of the histogram, according to the phase angle in the acoustic cycle. Thus, after a large amount of acoustic cycles (around 500), the histogram forms a pattern of a modulated DSD. Since accounting for a large amount of acoustic cycles (to emulate the PDPA/LDV measurement) in the CFD simulation is prohibitively expensive, our approach consisted in taking a small computational probe volume to construct the droplet size histograms in time, from the droplets (with their corresponding sizes) contained in such probe volume. The time series of histograms were phase averaged over four cycles.

Predictions of DSD modulation due to spray/acoustic interactions obtained by both EL and PMoM agree qualitatively with experimental observations, see Figure 16: With increasing amplitude of acoustic pressure oscillation, particle numbers at phase $\phi \approx \pi$ are reduced, while particle numbers at phases $\phi \approx 0$ and $\phi \approx 2\pi$ are increased. This modulation pattern is clearly more pronounced at larger oscillation amplitudes, while it does not vary strongly with particle size. A one-to-one quantitative comparison of experimental and computational results is not possible, because as noted above particle counts that can easily be realized in experiment are inaccessible to CFD simulations. Thus, the actual particle counts in experiment and EL differ by more than an order of magnitude. Furthermore, the EL results exhibit non-negligible statistical variance due to the small particle counts. The pMoM results, on the other hand, show by design no statistical fluctuations. Nonetheless, the CFD results support the conclusion that the mechanism described in "Modulation of the DSD" section is responsible for the clustering effect evidenced in the experiment.

Conclusions

CFD methods have been employed in this work to describe the spray response to an acoustic field. Two important kinds of spray response, AA and ND wave formation, have been identified and characterized. The acoustic displacement ($\hat{u}_c/\lambda f$) and mean flow velocity ($\hat{U}_c$) have been found to be important parameters of classification. The mechanisms producing these two kinds of spray response have been presented and the role of system parameters has been discussed for each one. Additional consequences of the ND wave formation for poly-disperse spays, such as modulation of the DSD, and distortion due to phase lags, have been also presented. A cross validation of the EL and EE spray descriptions was carried out, with the spirit of evaluate the capabilities of the cost-effective PMoM approach and exploring its limits. The need of a correction schema of the relaxation approach for large particle sizes, called here *relaxation approach with limited inertia* has been recognized, formulated and investigated.

The hypothesis that the effect of ND wave formation is the dominant mechanism in the experimental configuration of Gurubaran and Sujith[2] has been validated successfully. Potential aspects to be investigated in the future include the assessment of more sophisticated methods to estimate the size–velocity correlation in the EE context, for oscillating flows in particular.

Notes

a. A Lagrangian time step to resolve the ODEs for the particles motion is denoted as Δt_L and should be shorter than Δt_E.
b. For a non-evaporative spray without break-up nor coalescence.
c. The number is in principle arbitrary but provides a minimal good population response statistics.
d. This is a post-processing step as all statistical information is known in the Lagrangian simulation.

e. Corresponding to an air flow rate of 10 L/min and a water flow rate of 25cm^3/min.

References

1. Katoshevski D, Ruzal M, Shakked T, et al. Particle grouping, a new method for reducing emission of submicron particles from diesel engines. *Fuel* 2010; 89: 2411–2416.
2. Gurubaran R and Sujith RI. An experimental investigation of non-evaporative sprays in axial acoustic fields. AIAA number 2008-1046, 2008.
3. Sujith R. An experimental investigation of interactions of sprays in acoustic fields. *Exp Fluids* 2005; 38: 567–587.
4. Gajan P, Strzelecki A, Platet B, et al. Investigation of spray behaviour downstream of an aeroengine injector with acoustic excitation. *J Propul Power* 2007; 23: 390–397.
5. Gurubaran R and Sujith RI. An experimental investigation of evaporative sprays in axial acoustic fields. AIAA number 2008-4769, 2008.
6. Chisty W, Vandsburger U, Saunder W, et al. Interaction between thermoacoustic oscillations and spray combustion. *Eng Turbul Model Exp* 2005; 6: 865–874.
7. Giuliani F, Gajan P, Diers O, et al. Influence of pulsed entries on a spray generated by an air-blast injection device: an experimental analysis on combustion instability processes in aeroengines. In: *Proceedings of the combustion institute*, vol. 29, Pittsburgh: The Combustion Institute, 2002, pp. 91–98.
8. Katoshevski D, Dodin Z and Ziskind G. Aerosol clustering in oscillating flows: mathematical analysis. *Atomizat Sprays* 2005; 15: 401–412.
9. Katoshevski D, Shakked T, Sazhin S, et al. Grouping and trapping of evaporating droplets in an oscillating gas flow. *Int J Heat Fluid Flow* 2008; 29: 415–426.
10. Clift R, Grace JR and Weber ME. *Bubbles, drops and particles*. New York: Dover Publications, Inc, 1978.
11. Carneiro J. *Development of a presumed function method of moments with applications to polydispersed sprays*. PhD Thesis, Technical University Munich, Garching, Germany, 2011.
12. Carneiro J, Dems P, Kaufmann V, et al. Eulerian simulations of polydisperse flows using a moments model with a relaxation approach for the moment transport velocities. In *7th international conference on multiphase flow, ICMF 2010*, Tampa, FL, 30 May–4 June 2010.
13. Dems P. *On Eulerian-Eulerian Large Eddy simulation of polydispersed, reacting spray flows with moment methods*. PhD Thesis, Technical University Munich, Garching, Germany, 2014.
14. Dems P, Carneiro J and Polifke W. Large eddy simulation of a particle-laden swirling flow with a presumed function method of moments. *Progr Comput Fluid Dyn* 2012; 12: 92–102.
15. Madsen R. *Computational and experimental study of sprays from the breakup of water sheets*. PhD Thesis, Group for Chemical Fluid Flow Processes, Esbjerg Institute of Technology, Aalborg University Esbjerg, Denmark, 2006.
16. Ferry J and Balachandar S. A fast Eulerian method for disperse two-phase flow. *Int J Multiphase Flow* 2001; 27: 1199–1226.
17. Ran W and Saylor JR. Improved particle scavening by a combination of ultrasonics and water sprays. *J Aerosol Sci* 2014; 67: 104–118.
18. Sujith R, Waldherr G, Jagoda J, et al. A theoretical investigation of the behavior of droplets in axial acoustic fields. *J Vib Acoust* 1999; 121: 286–294.
19. Polifke W, Wall C and Moin P. Partially reflecting and non-reflecting boundary conditions for simulation of compressible viscous flow. *J Comput Phys* 2006; 213: 437–449.
20. Bo Y and Watkins P. Mathematical development and numerical analysis of further transport equations for the droplet size moment theory. In: *19th annual meeting of ILASS-Europe*. Nottingham, UK: Institute for Liquid Atomization and Spray Systems, 2004.
21. Gurubaran K. *Behaviour of sprays in acoustic fields*. PhD Thesis, Department of Aerospace Engineering, Indian Institute of Technology Madras, India, 2009.

Appendix I

Notation

Greek symbols.

α	droplet volume fraction
γ	density ration between droplet/gas
Γ	gamma function
κ	parameter of particle-size/-velocity correlation
λ	acoustic wave length
ν	kinematic viscosity
ρ	density
τ	relaxation time of particles/moments
τ_c	stress tensor
ϕ	phase angle
ω	frequency of oscillation (in radians/s)

Latin symbols

c	speed of sound
C_0	shape parameter of Gamma function
C_D	drag coefficient
D	droplet diameter
D_{32}	Sauter mean diameter
e	Euler's number
f	frequency of oscillation
$f(D)$	number density function (w.r.t. diameter D)
g	gravitational acceleration
M	momentum source term
$M^{(k)}$	k-th Moment of number density function
M_a	acoustic Mach number
N^+	set of positive integer numbers
n_p	number of particles

p	shape parameter of Gamma function	V	control volume
P	pressure	We	Weber number
q	shape parameter of Gamma function	x	x-coordinate
Re_p	particle Reynolds number		
S	integral drag term in disperse phase momentum equation		

S_t Stokes number, i.e. ratio of particle relaxation time to oscillation period

t time

u velocity

$u^{(k)}$ transport velocity of k-th moment

$\hat{U}_c$ time average ("mean") of forcing velocity

Sub-/superscripts.

$'$ oscillatory component (deviation from time average)

c   continuous phase

p   particle (discrete) phase